Correlation effects in neon studied by elastic and inelastic high-energy electron scattering

J. J. McClelland and M. Fink
Physics Department, The University of Texas at Austin, Austin, Texas 78712
(Received 16 March 1984)

The elastic and inelastic differential cross sections of 35-keV electrons incident on Ne were measured in the momentum-transfer range of 1—10 a.u. (20—200 mrad). The accuracies maintained throughout the experiment were 0.2% for the elastic scattering intensities and 2″ for the scattering angles. The diffraction unit is discussed. The elastic data are compared with partial-wave cross sections based on several atomic wave functions (Hartree-Fock, configuration-interaction, and independent-electron-pair approximation). None of the theoretical results coincides with the data within the error limits over the whole measured angular range. The large-angle results show very small deviations from the calculated cross sections and so this range is used to bring the measured cross sections to an absolute scale. The elastic, inelastic, and total cross sections were integrated and several potential energies were evaluated. The differences between the measured potential energies and the Hartree-Fock results reveal the importance of correlation for the electron-nuclear potential V_{ne} and the electron-electron potential V_{ee} which in turn can be decomposed into V_{ee}(Coulomb) and V_{ee}(exchange) parts.

I. INTRODUCTION

In the past 15 years there have been significant advances made in the calculation of atomic and molecular wave functions. Inclusion of correlation effects has recently become more and more feasible with the improvement of high-speed computation facilities. These new theoretical results have led to increased interest in experimental verification of the calculated wave functions with particular emphasis on the attempts to include correlation. The standard benchmarks, such as the total energy of the system, the dipole moment, and the equilibrium internuclear distances in a molecule do provide a check of whether the correlation is properly taken into account, but they allow only limited conclusions from comparisons. Being just a single number (or at best a few numbers), these quantities cannot contain full information on the wave function. Experimental techniques which probe the entire wave function are clearly superior if the most rigorous test is to be applied to theory.

One such type of experiment is high-energy electron scattering. Within the framework of the first Born approximation, total, elastic, and inelastic scattering intensities can be related to the target wave function by the Fourier transform of the first- and second-order charge densities. Recent advances in the technology of high-energy electron scattering have made it possible to measure cross sections with an accuracy of 0.2%. This has opened new possibilities for accurate investigations which emphasize the correlation effects in the wave function. By subtracting theoretical scattering intensities based on a Hartree-Fock (HF) wave function from measured cross sections, one can create a difference curve (referred to as "$\Delta\sigma$ curve") which shows how the true wave function differs from the HF. Plotting the analogous difference calculated from theoretical correlated scattering intensities and the HF theory provides a comparison which shows how far the new wave function has come towards a true representation of the atom or molecule in question.

With regards to correlation, neon has been the subject of a number of theoretical studies, as well as a few experimental investigations. As a ten-electron closed-shell system, it provides a good study case, having enough electrons to prove challenging for a theoretical investigation, but not enough to have particularly large relativistic effects. Being an inert gas with a fairly large nuclear charge, it is also an excellent scattering target for electron diffraction.

Several Hartree-Fock calculations, both relativistic and nonrelativistic, have been carried out for neon,[1] with the basic result that the nonrelativistic HF energy is -128.547 a.u.[2] (1 a.u.$=27.2107$ eV), the relativistic correction being -0.131 a.u.[3] Spectroscopic results of very high accuracy are also available,[4] giving the total experimental energy of the neon atoms as -129.056 a.u. When one takes into account a contribution of $+0.009$ a.u. from the Lamb shift,[3] the net correlation effect (nonrelativistic "true" energy minus nonrelativistic HF energy) is estimated to be -0.383 a.u. (10.4 eV).

Several attempts have also been made to calculate a correlated wave function for neon. The basic approach of a more or less standard configuration-interaction (CI) expansion has been taken by Bunge and Peixoto,[5] and Tanaka and Sasaki,[6] while an IEPA (independent-electron-pair approximation), or Bethe-Goldstone approach has been employed by Naon and Cornille,[7] using the method of Nesbet.[8] Bunge and Peixolo's calculation has been hampered by the fact that full CI was not possible. Tanaka and Sasaki considered only L-shell correlation and reproduced slightly more than half the total correlation energy, while Bunge and Peixoto, using a 231-term expansion, achieved about 85% of the energy. (Only a 65-term Ne wave function was used for the calculation of the electron scattering factors. The total energy was 128.860 25 a.u.)

In contrast, Naon and Cornille reproduced 97% of the correlation energy using IEPA.

So far there have been only two experimental investigations of correlation effects in the neon wave function using high-energy electron scattering. Fink and Moore[9] measured total differential electron scattering at 40 keV, and Duguet, Lahmam-Bennani, and Rouault[10] measured elastic and inelastic electron scattering separately at 25 KeV. The results of Fink and Moore[9] agreed well with the $\Delta\sigma$ curve calculated by Naon and Cornille, and slightly worse with a 65-term truncated version of Bunge and Peixoto's original calculation.[11] The results of Duguet *et al.*[10] also support the IEPA calculation; in fact, the elastic and inelastic scattering both show good agreement individually. It is noteworthy, however, that Born-approximation scattering intensities were used to put the elastic data onto an absolute scale and in creating the $\Delta\sigma$ curve. This procedure requires the validity of the first Born approximation to the level of the experimental uncertainties.

II. THEORY

As used in this work, the definition of the $\Delta\sigma$ curve, in atomic units, is as follows:

$$\Delta\sigma=\frac{K^4}{4}(I^{\exp}-I^{\mathrm{HF}}) , \tag{1}$$

where K is the momentum transfer $(4\pi\lambda^{-1})\sin(\theta/2)$, λ is the relativistic De Broglie wavelength, θ is the scattering angle, $I^{\exp}$ represents either the elastic, inelastic, or total experimental intensity, and I^{HF} is a theoretical intensity derived from a Hartree-Fock atomic wave function. If the Born approximation holds, the elastic and inelastic scattering intensities in Eq. (1) can be written as

$$I_{\mathrm{el}}=4K^{-4}[Z-F_x(K)]^2 \tag{2}$$

and

$$I_{\mathrm{inel}}=4K^{-4}S_x(K) , \tag{3}$$

where $F_x(K)$ and $S_x(K)$ are the x-ray coherent and incoherent scattering factors. The K values for the inelastic scattering have been corrected as outlined in Ref. 12 (Chap. 5, Eq. 5.7). It is through these relations that the connection with the target wave function is made, since the x-ray scattering factors are directly related via Fourier transformations to the one- and two-electron charge densities.[12] In the incident energy range used in the present experiments it is well known[12] that the Born approximation deviates from experiment by (1—3)%. Since the correlation effect in a target wave function causes changes in the scattering intensities of similar (or even smaller) magnitude, it might seem that any difference between experiment and theory displayed in the $\Delta\sigma$ curve would arise from a conglomeration of correlation effects and Born-approximation shortcomings. This problem can be avoided by calculating the HF intensity from a partial-wave (PW) expansion. In fact, all processes which begin to degrade the validity of the relations (2) and (3), such as spin flip, exchange, and relativistic effects, can be included in the HF intensity used to create the $\Delta\sigma$ curve. If this is done, these effects will be canceled (to first order) in the resulting difference. This can be seen by considering the following argument. Suppose the partial wave scattering intensity is related to the Born intensity by a factor $R(K)$, whose value differs from 1 only by a few percent,

$$I_{\mathrm{PW}}(K)=R(K)I_{\mathrm{Born}}(K) . \tag{4}$$

Assuming $R(K)$ is the same for both a correlated atom and a HF atom, the difference in intensities become

$$\Delta I_{\mathrm{PW}}(K)=R(K)\Delta I_{\mathrm{Born}}(K) . \tag{5}$$

Thus ΔI is the same for Born theory and PW theory, within the factor $R(K)$, which is near unity. If, however, one were to subtract a Born-HF theory from a PW correlated intensity, the result would be

$$I_{\mathrm{PW}}-I^{\mathrm{HF}}_{\mathrm{Born}}=R\Delta I_{\mathrm{Born}}+(R-1)I^{\mathrm{HF}}_{\mathrm{Born}} . \tag{6}$$

Since ΔI_{Born} is usually only a few percent of I_{Born}, the second term on the right-hand side of Eq. (6) can easily be as big as or even bigger than the first term. Hence if one treats the data according to Eq. (5) and not (6), the interpretation of the results in terms of the Born approximation is justified, allowing direct comparison with theoretical $\Delta\sigma$ curves calculated strictly in the Born approximation.

When elastic and total data are collected separately, three individual $\Delta\sigma$ curves can be constructed: $\Delta\sigma^{\mathrm{tot}}$, $\Delta\sigma^{\mathrm{el}}$, and $\Delta\sigma^{\mathrm{inel}}$. Before subtracting theory from experiment it is necessary to put the elastic and total intensities on an absolute scale, since they are provided by the experiment only within a constant factor. This is done by matching (via least squares) the elastic data to partial wave scattering cross sections, or the total data to the same intensities plus Born-approximation inelastic intensities. Once elastic and total $\Delta\sigma$ are produced, the inelastic one can be created by simple subtraction. This should be a valid approach if the matching is carried out properly.

In all systems studied so far, correlation effects have been limited to small angle scattering, so there is always a K value (typically around 4—5 a.u.) above which the $\Delta\sigma$ curve is essentially flat and available for matching. Actually, this can be explained intuitively, in that correlation has an effect on the wave function mostly in the outer filled electron shells. Since large angle scattering is dominated by the Coulombic field near the nucleus, one would expect the electronic screening to be weak, and agreement with HF above a certain K value should be good.

Electron scattering results are not only limited to displaying correlation effects in the Fourier-transform space of the wave function. Energy relations can also be derived, in which correlation energies are obtained from integrals over the elastic, inelastic, and total $\Delta\sigma$ curves. The effect of correlation on the electron-nuclear potential, which is called ΔV_{ne}, and the same quantity for the electron-electron potential (ΔV_{ee}) can be extracted from elastic and inelastic data, respectively, by noting the definitions (Ref. 12, p. 114)

$$V_{ne} = -Z \int \frac{\rho(\mathbf{r})}{r} d\mathbf{r} , \tag{7}$$

$$V_{ee} = \tfrac{1}{2} \int \frac{\rho_c(\mathbf{r})}{r} d\mathbf{r} \tag{8}$$

(atomic units are used). It can be shown that integrating the x-ray form factor $F_x(K)$ over K yields the same result as Eq. (7) within a constant:

$$\int F_x(K) dK = \frac{\pi}{2} \int \frac{\rho(\mathbf{r})}{r} d\mathbf{r} = -\frac{\pi}{2Z} V_{ne} . \tag{9}$$

Similarly, V_{ee} can be related to the incoherent x-ray scattering factor $S_x(K)$ by

$$\int [S_x(K) - Z + F_x^2(K)] dK = -\pi V_{ee} . \tag{10}$$

Sometimes V_{ee} is broken down into two parts, a Coulomb part V_{ee}^{Coul} and an exchange part V_{ee}^{exch}:

$$V_{ee}^{\text{Coul}} = -\frac{1}{\pi} \int F_x^2(K) dK \tag{11}$$

and

$$V_{ee}^{\text{exch}} = -\frac{1}{\pi} \int [S_x(K) - Z] dK . \tag{12}$$

All these relations can be combined to show that the correlation effect on each of the three types of potential energy can be derived from electron scattering data, using the first Born expressions (2) and (3),

$$\Delta V_{ne} = -\frac{2Z}{\pi} \int \Delta F_x(K) d(K)$$

$$= -\frac{Z}{\pi} \int K^2 [(I_{\text{el}}^{\text{exp}})^{1/2} - (I_{\text{el}}^{\text{HF}})^{1/2}] dK , \tag{13}$$

$$\Delta V_{ee}^{\text{Coul}} = \frac{1}{\pi} \int \Delta\sigma^{\text{el}}(K) dK + \Delta V_{ne} , \tag{14}$$

$$\Delta V_{ee}^{\text{exch}} = \frac{1}{\pi} \int \Delta\sigma^{\text{inel}} dK . \tag{15}$$

Adding Eqs. (13) and (14) shows that the total correlation energy can be extracted from the total $\Delta\sigma$ curve:

$$\Delta E_{\text{corr}} = \tfrac{1}{2} \Delta V_{\text{tot}} = \frac{1}{2\pi} \int \Delta\sigma^{\text{tot}} dK . \tag{16}$$

This relation is often referred to as Tavard's theorem.[13]

III. EXPERIMENTAL APPARATUS

A new diffraction unit was built which resembled in many aspects the unit described in detail in Ref. 9. Here only those elements will be discussed which have been modified or have been added. An overview of the apparatus is shown in Fig. 1.

A. General considerations

The vacuum chamber is of all-aluminum construction. The main pumping is done with a 12-in. diffusion pump equipped with a freon cooled trap. An auxiliary 14-in. diffusion pump is placed directly under the gas nozzle and is fitted with a cone-shaped baffle reaching to within 1 cm of the nozzle tip. Typically, with a cone opening of 3 cm,

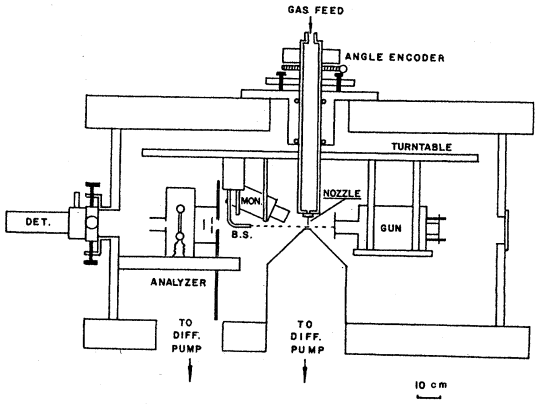

FIG. 1. High-energy elastic electron scattering apparatus (side view).

the chamber pressure rises about 1.6×10^{-7} Torr per Torr of pushing pressure.

During the experiments on neon (pushing pressure 14.6 Torr), the total pressure in the chamber can be calculated to be 4.9×10^{-6} Torr. As will be discussed later, this background pressure does cause some, albeit very little, background scattering and must be compensated for when very high-accuracy data are desired. It should be noted, however, that this level of background represents a significant improvement over our previous electron-diffraction system. The magnetic field was compensated below 1 mG in the volume crossed by the electrons.

B. Gas-flow system

The purpose of the gas-flow system is to provide a well-regulated flow of gas through the nozzle at pressures ranging from 1 to about 20 Torr. The regulation consists of a Veeco PV-10 piezoelectric valve and an MKS Baratron differential manometer connected on one side to a reference volume. A reservoir connected to the other side of the manometer is maintained, via a feedback connection to the PV-10 valve, at a fixed pressure of a few hundred Torr. A small amount of gas is allowed to flow continuously from the reservoir through a 12×0.004-in.^{2}-i.d. capillary into the region behind the nozzle, where a pressure of a few Torr is maintained. The expansion through the long capillary minimizes the Joule-Thompson cooling and provides a very stable flow rate. The nozzle itself is a 304 stainless-steel 22 gauge hypodermic needle of 3-cm length.

C. Turntable and angle measurement

The turntable, on which the electron gun, the monitor, the gas nozzle, and the beam stop are mounted, consists of a 3×140-cm^2 aluminum disk suspended from the lid of the chamber on two tapered roller bearings. The angular measurement is done with an Itek Digisec high-resolution angle encoder coupled directly to the turntable shaft. This encoder has a resolution of 2^{19}-1 bits per circle (or 2 arc sec) and provides absolute angular position informa-

tion by supplying pulses on dedicated lines for clockwise and counterclockwise motion recorded by an up-down counter.

D. Electron gun

The electron gun being of the Steigerwald telefocus[14] type, provides a 35-keV beam of electrons of full width at half-maximum (FWHM) 0.5 mm, with currents variable from 0.01 to 25 μA.

The beam stop (BS), which traps effectively more than 99% of the incident electrons is of the "Wood's-horn" type, consisting of a bent brass tube 0.125 in. in diameter.

The gun control is of the standard self-biasing type. With this setup the electron-beam current has been stable for periods of weeks, with no detectable drift in position or intensity.

E. Möllenstedt analyzer

The Möllenstedt electron-energy analyzer, first developed by Möllenstedt in 1949,[15] is essentially a cylindrical electrostatic einzel lens of very strong power. Such a configuration leads to very high chromatic aberration for off-axis rays, causing dispersion of the electrons according to their energy. This dispersion can be utilized for energy analysis. In fact, with entrance and exit slits placed appropriately, and with suitable slit openings, resolution of better than 0.5 eV at 35 keV can be obtained. The resolution obtainable for the analyzer and 35 keV electrons was measured to be 23 meV.[16]

Detailed experimental investigations as well as theoretical analyses (including line-charge models and numerical-ray tracing) of the Möllenstedt analyzer have been carried out.[15–20] The analyzer used in the experiments described in this work was made after the design of Wellenstein.[19] It consists of a pair of stainless-steel 0.375-in.-diam rods mounted with a separation of 0.285 in. on a high-voltage insulator at the center of an aluminum $5\times10\times13$-in.^{3} housing. Entrance and exit apertures are cut in the walls, and an adjustable (width and position) slit is placed in front. Adjustment is achieved by means of small motors. The detector slit assembly, mounted on the outside wall of the chamber, is movable horizontally and vertically and consists of a vertical and a horizontal slit, each adjustable with a micrometer. In addition, the detector and entrance slits can both be rotated to compensate for a possible small tilt in the rods.

Angular acceptance of the Möllenstedt analyzer is not as large as that of a cylindrical 127° or hemispherical analyzer, and it must be carefully considered, especially in experiments such as the ones described here, where the entire scattering volume must be seen by the detector in order to avoid false angular dependence in the scattering cross section. As evidenced by the plot of the measured angular dependence of the position of the caustic, shown in Fig. 2, there is limited angular focusing in the caustic region, which is caused by the fact that both positive and negative entrance angles result in trajectories on the energy-loss side of the central ray. This causes a finite source of monochromatic electrons placed symmetrically in front of the analyzer entrance slit to have its center at one edge of the image in the detector plane (corresponding to the caustic), while both edges are folded onto each other on the energy-loss side of the caustic, with an extent roughly proportional to the square of the source angle. Note that a change of the position of the caustic is equivalent to a change in the electron energy. This has the consequence that if one considers a very-high-resolution spectrum at a small scattering angle, the resolution will appear to deteriorate slightly as the angle is increased, due to the fact that the angle subtended by the scattering volume gets larger as the scattering angle increases, causing the effective source size to grow.

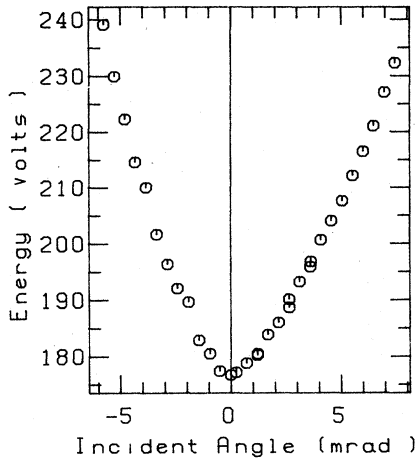

FIG. 2. Dependence of the caustic of a Möllenstedt analyzer as a function of the electron energy and the entrance angle of the electrons with the vertex at the entrance slit (dispersion curve).

One more advantage of the Möllenstedt analyzer which should be mentioned is the ease with which it can be converted to measure the total (elastic plus inelastic) differential cross section. One needs only to ground the rods and move the detector to the center. After minor adjustments to the slit widths (if necessary), a total measurement can be made directly consequent to an elastic one.

The electronics used to control the electron gun and Möllenstedt analyzer are housed in two insulated metal enclosures. High voltage is supplied to both the gun and the analyzer by a precision regulated Spellman RHSR60N60 power supply. In this arrangement, any small fluctuations in the high voltage are canceled to first order since they are applied simultaneously to the electron gun and the analyzer. Floating at high voltage are a Fluke model 40/DR power supply and an Interstate F-72 function generator. The voltage (typically $+250$ V) from the Fluke power supply is connected through a voltage divider to the electron gun. This voltage divider, calibrated in steps of 10 V, allows the voltage difference between the analyzer rods (connected directly to the high voltage) and the gun to be varied in a well-defined way, in order to help find the caustic and also calibrate the energy-loss

spectra.

IV. RESULTS

The data-reduction techniques used in this work are exactly the same as those used in previous high-energy electron scattering work at the University of Texas; for more details the reader is referred to Ref. 21. The results of the present investigation are shown in Figs. 3–7. All data sets were collected with 34 786-eV incident electrons. Energy calibration was accomplished by performing electron diffraction on N_2 with the same experimental setup—the energy which resulted in a bond length $[r_g(1)]$ of 1.0976 Å was used.

Figure 3 shows the total measurement, composed of several sets each providing two sides of data measured with 300 sec per point. The HF cross sections used in producing the experimental $\Delta\sigma$ are the sum of elastic and inelastic contributions. The elastic contribution contained relativistic partial wave scattering factors[22] (corrected for exchange[23]), calculated from the relativistic HF wave function of Mann.[24] The inelastic portion was made up of the HF incoherent scattering factors of Tavard *et al.*[25] Matching between experiment and theory was performed from $K=7$ to 11 (a.u.), in the region where the curve is flat. In Fig. 4 are shown the elastic results, consisting of three data sets of two sides each (two sets had 300 sec per point, one had 100 sec per point). The same theory as mentioned above was used, with the exception that the inelastic factors were left out. In this case matching was limited to the range $K=3$ to 7 (a.u.), because this is the only true flat region of the curve. In order to emphasize the small size of the effect being measured, a marker is drawn in Fig. 4 indicating ±0.2% of the scattering intensity. Figure 5 shows the same data transformed into a ΔF_x curve, by means of Eq. (13). This function is used to evaluate Eq. (13) and is provided for future comparison with x-ray data, should they become available.

As an illustration of the dramatic effects introduced by assuming the Born approximation at the wrong stage, the exact same data as shown in Fig. 4 was used to create a $\Delta\sigma$ curve where the theory contained Born amplitudes obtained from Hubbell's relativistic HF x-ray scattering factors.[1] The results are shown in Fig. 6 (matching was carried out with the average ratio of the countrates and the theory utilizing the whole K range in this case). The significant difference between Figs. 4 and 6 indicates that considering the high level of precision available in this experiment it is very important that all relativistic, partial wave, and exchange effects be included in the theory used for the $\Delta\sigma$, so that the difference can only be attributed to correlation. It should be borne in mind at the same time, though, that the maximum deviation of the curve in Fig. 6 at $K=10$ (a.u.) corresponds to only about 1.3% of the raw intensity.

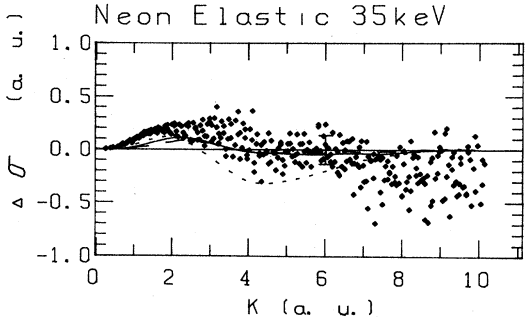

FIG. 4. Neon elastic $\Delta\sigma$ (partial-wave theory). Experiment (◇); 65-term CI (——); L-shell CI (— — —); IEPA, Bethe-Goldstone (---). A marker is drawn as $s=6$ a.u. indicating ±0.2% of the scattering intensity.

The inelastic $\Delta\sigma$ curve was obtained by fitting a 10th order polynomial to the elastic $\Delta\sigma$ and subtracting from the total, as discussed in Sec. II. This method was used because of the need for interpolation and the reduction in scatter which resulted. The inelastic results are shown in Fig. 7.

Shown also in Figs. 3–7 are theoretical $\Delta\sigma$ curves calculated by subtracting Born-approximation HF nonrelativistic scattering intensities from equivalent CI intensities. The HF cross sections were obtained from the x-ray coherent and incoherent scattering factors tabulated by Hubbell *et al.*[26] using Eqs. (2) and (3) while the CI intensities were calculated from the $F_x(K)$ and $S_x(K)$ values

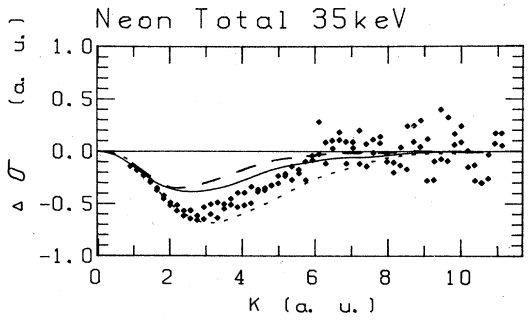

FIG. 3. Neon total $\Delta\sigma$. Experiment (◇); 65-term CI (——); L-shell CI (— — —); IEPA, Bethe-Goldstone (---).

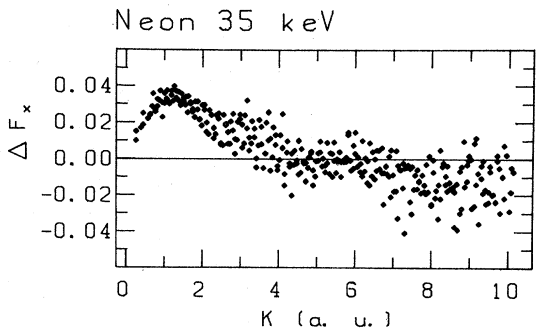

FIG. 5. Neon ΔF_x curve.

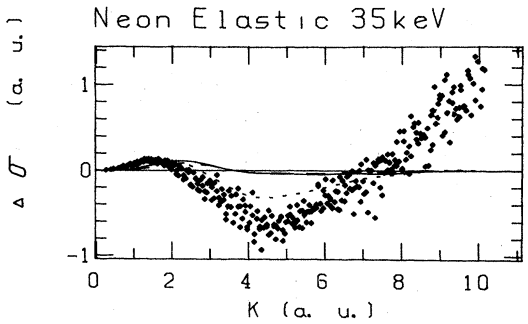

FIG. 6. Neon elastic $\Delta\sigma$ (born theory). Experiment ($\Diamond$); 65-term CI (——); L-shell CI (— — —); IEPA, Bethe-Goldstone (---).

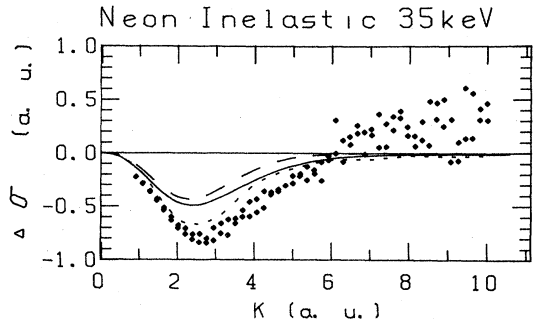

FIG. 7. Neon inelastic $\Delta\sigma$. Experiment ($\Diamond$); 65-term CI (——); L-shell CI (— — —); IEPA, Bethe-Goldstone (---).

presented by Peixoto, Bunge, and Bonham,[11] Tanaka and Sasaki,[6] and Naon and Cornille.[7]

In agreement with the previous experimental results of Duguet *et al.*[10] and Fink and Moore,[9] the new total $\Delta\sigma$ appears to favor the IEPA calculation, lying somewhat lower than the CI predictions. This is perhaps not surprising, since the shape of all the curves is roughly the same and the integral under the curve should yield the total correlation energy [see Eq. (16)], which is better reproduced by the Naon and Cornille results.

On the other hand, the opposite seems to be the case for the elastic $\Delta\sigma$. Figure 4 shows that the data lacks the minimum around $K\simeq 4.5$ which is evident in the IEPA calculation, and tends to follow the trend indicated by the CI theories. We note in passing that if the somewhat more noisy data from $K=7$ to 10 is included in the matching process the discrepancy between the data and the IEPA becomes larger, and the integration under the curve yields an unreasonably large number for ΔV_{ne}, so this region was excluded. If one were to consider Fig. 6 instead of Fig. 4, however, the indication would be that the IEPA calculation does better, since the minimum at $K\simeq 4.5$ becomes quite visible when pure Born theory is used to produce the $\Delta\sigma$. It is interesting yet unfortunate that the use of pure Born theory with experimental data introduces the same qualitative behavior into the $\Delta\sigma$ curve that the IEPA theory predicts, leading to erroneous conclusions. In the small-K range it appears that the IEPA calculation predicts the slope of a $\Delta\sigma$ better than the two CI calculations. However, the lack of some correlation in the CI results makes this disagreement not too surprising. The basis for this is that the missing contributions to the correlation in the CI modify the electron density mainly at the large atomic distances.

The inelastic results, as shown in Fig. 7, agree more with the IEPA calculation than with the CI. This is in accord with the total but in contrast to the elastic results—a situation which is understandable since the inelastic data are derived from the total by subtracting the essentially flat elastic $\Delta\sigma$. Again, the total correlation energy comes into play in dictating the need for a sufficiently large area under the curve to reproduce the needed value.

As discussed in Sec. II [Eqs. (13)—(16)], it is also possible to derive potential-energy quantities from the $\Delta\sigma$ curves by integrating over K. These results are shown in Table I, along with equivalent values from the literature. Although the errors are large, it can still be said that the tendency is to favor the CI calculations over the Bethe-Goldstone, the trend being towards a small positive ΔV_{ne}

TABLE I. Correlation effects of potential-energy quantities (all numbers of eV).

	ΔE_{tot}[a]	ΔV_{ne}	ΔV_{ee}	$\Delta V_{ee}^{\text{exch}}$	$\Delta V_{ee}^{\text{Coul}}$
This work	−8.6±2	+5.7±8	−22.4±8	−14.2±8	−8.2±8
Duguet *et al.*	−7.5±7	−7.3±7	−7.6±7	−7.9±7	−0.2±7
65-term CI	−6.7[b]	+3.8	−17.2	−13.9	−3.3
L-shell CI	−4.7[b]	+2.3	−11.7	−9.7	−2.0
Bethe-Goldstone	−12.4[b]	−6.2	−18.6	−17.2	−1.4
Z expansion	−10.5	+1.4	−22.3		

[a]Note $\Delta E_{\text{tot}}=\frac{1}{2}\Delta V_{\text{tot}}$.

[b]These numbers were calculated by integrating the total $\Delta\sigma$ curves. Unfortunately they do not all agree with the correlation energies claimed for the wave functions: 8.9 eV for the 65-term CI, 5.8 eV for the L-shell CI, and 10.2 eV for the IEPA.

and a large negative ΔV_{ee}. This trend is also exhibited by the Z-expansion results of Goruganthu and Bonham,[27] shown in the last row of Table I. Since these numbers are derived from spectroscopic results and do not rely on an *ab initio* wave-function calculation, they provide an independent check for the separation of the potential into its components.

All integral quantities and electron-diffraction data derived from and shown in Table I depend critically on the quality of the measurements at large-k values. In spite of the fact that the present data present accumulated counts in excess of 10^6 and thus the statistical uncertainty is less than 0.1%, in spite of the fact that the finite size of the atom and electron beam do not modify the cross sections,[28] and in spite of the fact that all important experimental parameters are monitored to ensure long-term stability to better than 0.1%, the matching process introduces sufficient ambiguities to cause uncomfortably large errors in the potential quantities. The error limits shown in Table I represent variations which occurred as matching was performed over different K ranges, as well as an estimation of the error introduced by the statistical noise in the data. With the present level of accuracy in the experiment, these numbers can only serve to indicate trends, despite some surprisingly good agreements (viz., ΔV_{ee} with Z expansion). They do provide good information, however, when taken in conjunction with the $\Delta\sigma$ curves. The disagreement between the present data and the values quoted by Duguet *et al.*[10] are based on the same problem. The noise of the previous measurements is about 10 times larger for k values past 5 a.u. The matching becomes more uncertain and it is very hard to ascertain quantitatively the error propagation to the integral quantities. Their quoted numbers refer only to the statistical uncertainties and neglect all systematic contributions.

V. CONCLUSION

In summary, the total $\Delta\sigma$ curve and its integral ΔE_{tot} are in agreement with the previous measurements of Duguet *et al.* and Moore and Fink, as well as with Bethe-Goldstone (or IEPA) calculations and Z-expansion results. The elastic $\Delta\sigma$ curve and its integral quantities ΔV_{ne} and $\Delta V_{ee}^{\text{Coul}}$ tend to favor CI calculations and Z-expansion predictions in contrast to the results of Duguet *et al.*,[10] which indicate a preference for Bethe-Goldstone. This discrepancy is explained as arising from inappropriate use of the Born approximation. The inelastic $\Delta\sigma$ derived from the total also shows agreement with IEPA calculations.

From these results, one can conclude that with regards to the portion of the wave function probed by inelastic scattering, the Bethe-Goldstone approach provides a better approximation than a limited CI calculation. Since the major contributor to the total $\Delta\sigma$ comes from the inelastic portion, total results show similar agreement. Concerning the elastic $\Delta\sigma$ curve it is first noteworthy that the amplitude of the correlation effect is significantly smaller when compared with the inelastic one. This reconfirms the expectation that the HF approximation predicts rather well quantities relating to the first-order charge-density matrix. The small remaining deviation favors the IEPA in the very small-K range but the experimental $\Delta\sigma$ curve fails to follow the IEPA prediction at $K=3$–6 a.u. In this range the CI calculations are superior. This situation can be intuitively understood if one considers the nature of the IEPA approximation. Since it considers only correlation between pairs of electrons within a single orbital, it can be expected to do well in reproducing the electron pair distribution (or second-order charge density), at the expense of the first-order charge density, which is concerned with the disposition of the orbitals with respect to the nucleus.

This conclusion represents a major step forward in the detail with which calculated wave functions can be examined experimentally. As this is a result from a new apparatus, the refinements which are inevitable over the next few years should continue to provide more and more detailed results reducing the noise level in the $\Delta\sigma$ curves and hopefully providing smaller error limits for the potential-energy quantities.

ACKNOWLEDGMENTS

This work was supported in part by the National Science Foundation under Grant No. CHE-8307174 and by the Robert A. Welch Foundation (Houston, Texas). The authors are especially grateful for the valuable assistance of Dr. H. F. Wellenstein in the design, construction, setup, and calibration of the Möllenstedt analyzer.

[1]For a good bibliography of wave functions, see J. H. Hubbell and I. Overbo, J. Phys. Chem. Ref. Data **8**, 69 (1979).
[2]E. Clementi and C. Roetti, At. Data Nucl. Data Tables **14**, 177 (1974).
[3]A. Veillard and E. Clementi, J. Chem. Phys. **49**, 2415 (1968).
[4]R. Kelley and D. Harrison, Jr., At. Data **3**, 177 (1971).
[5]C. F. Bunge and E. M. A. Peixoto, Phys. Rev. A **1**, 1277 (1970).
[6]K. Tanaka and F. Sasaki, Int. J. Quantum Chem. **5**, 157 (1971).
[7]M. Naon and M. Cornille, J. Phys. B **5**, 1965 (1972).
[8]R. K. Nesbet, Rev. Mod. Phys. **35**, 522 (1963); Adv. Chem. Phys. **9**, 321 (1965).
[9]M. Fink and P. G. Moore, Phys. Rev. A **15**, 112 (1977).
[10]A. Duguet, A. Lahmam-Bennani, and M. Rouault, J. Chem. Phys. **79**, 2786 (1983).
[11]E. M. A. Peixoto, C. F. Bunge, and R. A. Bonham, Phys. Rev. **181**, 322 (1969).
[12]R. A. Bonham and M. Fink, *High Energy Electron Scattering* (Van Nostrand Reinhold, New York, 1974).
[13]C. Tavard, Cah. Phys. **20**, 397 (1965).
[14]K. H. Steigerwald, Optik **5**, 468 (1949).
[15]G. Möllenstedt, Optik **5**, 499 (1949).
[16]K. H. Gaukler, Z. Phys. **196**, 85 (1966).
[17]A. J. Metherell and M. J. Whelan, Br. J. Appl. Phys. **16**, 1038 (1965).
[18]A. J. Metherell and M. J. Whelan, J. Appl. Phys. **37**, 1737

(1966).
[19]H. F. Wellenstein, J. Appl. Phys. **44**, 3668 (1973).
[20]W. Lippert, Optik **12**, 467 (1955).
[21]M. Fink, P. G. Moore, and D. Gregory, J. Chem. Phys. **71**, 5227 (1979).
[22]A. C. Yates, Comput. Phys. Commun. **2**, 175 (1971).
[23]M. Fink and C. Schmiedekamp, J. Chem. Phys. **71**, 5243 (1979).
[24]J. B. Mann (private communication).
[25]C. Tavard, D. Nicolas, and M. Rouault, J. Chim. Phys. **64**, 540 (1976).
[26]J. H. Hubbell, W. J. Veigele, E. A. Biggs, R. T. Brown, D. T. Cromer, and R. J. Howerton, J. Phys. Chem. Ref. Data **4**, 471 (1975).
[27]R. R. Goruganthu and R. A. Bonham, Phys. Rev. A **26**, 1 (1982).
[28]M. Miller and M. Fink, J. Mol. Struct. **48**, 373 (1978).